APL Materials

Heat dissipation in partially perforated phononic nano-membranes with periodicities below 100 nm

Cite as: APL Mater. **10**, 051113 (2022); https://doi.org/10.1063/5.0091539
Submitted: 15 March 2022 • Accepted: 28 April 2022 • Published Online: 25 May 2022

Antonin M. Massoud, Valeria Lacatena, Maciej Haras, et al.

Heat dissipation in partially perforated phononic nano-membranes with periodicities below 100 nm

Cite as: APL Mater. 10, 051113 (2022); doi: 10.1063/5.0091539
Submitted: 15 March 2022 • Accepted: 28 April 2022 •
Published Online: 25 May 2022

Antonin M. Massoud,[1,2] Valeria Lacatena,[3,4] Maciej Haras,[3,4,a)] Emmanuel Dubois,[3] Stéphane Monfray,[4] Jean-Marie Bluet,[1,b)] Pierre-Olivier Chapuis,[2,b)] and Jean-François Robillard[3,b)]

AFFILIATIONS

[1] Univ Lyon, Institut des Nanotechnologies de Lyon (INL), CNRS, INSA de Lyon, F-69621 Villeurbanne, France
[2] Univ Lyon, CNRS, INSA-Lyon, Université Claude Bernard Lyon 1, CETHIL UMR5008, F-69621 Villeurbanne, France
[3] University Lille, CNRS, Centrale Lille, Junia, University Polytechnique Hauts-de-France, UMR 8520 - IEMN–Institut d'Electronique de Microélectronique et de Nanotechnologie, F-59000 Lille, France
[4] STMicroelectronics, 850, rue Jean Monnet, F-38926 Crolles, France

Note: This paper is part of the Special Topic on Phononic Crystals at Various Frequencies.

[a)] **Current address:** CENTERA Laboratories, Institute of High Pressure Physics PAS, Sokołowska 29/37, 01-142 Warsaw, Poland and Center for Advanced Materials and Technologies CEZAMAT, Warsaw University of Technology, Poleczki 19, 02-822 Warsaw, Poland.
[b)] **Authors to whom correspondence should be addressed:** jean-marie.bluet@insa-lyon.fr; olivier.chapuis@insa-lyon.fr; and jean-francois.robillard@iemn.fr

ABSTRACT

Understanding how thermal-phonon paths can be shaped is key for controlling heat dissipation at the nanoscale. Thermophononic crystals are periodic porous nanostructures with thermal conductivity deviating from effective medium theory, which is possible if the characteristic sizes are of the order of phonon mean free paths and/or if phonons are forced to flow in privileged directions. We investigate suspended silicon nanomembranes with a periodic array of partially perforated holes of original paraboloid shape, with all characteristic lengths below 100 nm. Results from scanning thermal microscopy, a thermal sensing technique derived from atomic force microscopy, indicate that partial perforation of the membranes impacts heat conduction moderately, with the holey crystals showing a thermal conductivity reduction by a factor 6 in comparison to the bulk and a factor 2.5 in comparison to the non-perforated membrane. The impact of the phononic shapes is analyzed in light of a complementary Monte Carlo ray-tracing estimate of the effective phonon mean free paths that include multiple phonon reflection and highlights phonon backscattering.

Blocking thermal phonons in confined geometries is a global strategy pursued by many groups in order to limit heat dissipation in crystalline materials. Configurations involving nanowires,[1] suspended membranes,[2,3] thin films,[4] superlattices,[5,6] or nano-constrictions[7,8] have been considered. Dispersion of low-thermal conductivity particles in a crystalline matrix is also an option and is usually known as nanocomposite.[9,10] Another key category of materials is based on phononic crystals (PnCs),[11,12] i.e., periodic arrays of inclusions or holes in 2D or 3D configurations, where reduction of apparent thermal conductivity by a factor larger than 10 was demonstrated.[13,14] The reason for the reduction is a ballistic transfer between boundaries of the material and constrictions of the flux path in the material between holes/inclusions, which both induce a decrease in local effective mean free paths (MFP). While there were originally some prospects for room-temperature coherent effect on thermal conductivity in such structures,[15–17] it is now well accepted that these effects manifest only at low temperature.[18,19] Typical phonon wavelengths are indeed usually lower than 10 nm at

room temperature, and coherent effects require, therefore, material's science bottom-up nanofabrication to control sizes in this regime close to ambient.[5,6]

At room temperature, understanding how phonon paths can be blocked efficiently for a given amount of matter is, therefore, a key issue.[20,21] It was shown that the surface/volume ratio is an important parameter for many geometries.[22] In addition, there are prospects that dendritic-like structures possess phonon-open channels while also holding "dead arms" where heat transport is mostly inefficient.[23] A drawback of these structures is their randomness. Here, we investigate partially perforated phononic membranes, which are 60 nm thin suspended membranes[24] with hole periodicities in the sub-100 nm regime,[25] i.e., well below the average mean-free path of silicon (close to 200 nm[4,26]). In contrast to previous studies,[2,27–29] the holes are not fully perforating the membranes and possess a paraboloid shape, with the maximal radius on the surface close to 20 nm. These novel structures may be more stable than fully perforated counterparts or could be filled at will. The original shapes complicate the Raman-thermometry analysis or other optics-based techniques as absorption may be non-homogeneous in the structures. As a result, we measure the thermal conductivity of these structures using scanning thermal microscopy (SThM).[30] The experimental results are compared to a ray-tracing estimation of frequency-dependent phonon mean free paths,[31] which accounts for multiple reflections and highlights phonon backscattering.

The suspended silicon membrane strips have a length of 200 μm, a width of 10 μm, and a thickness t measured close to 60 nm as in Ref. 24 [see Fig. 1(a) for a cross-sectional schematic and Fig. 1(b) for a top view]. The fabrication process flow[25,32] is illustrated in the supplementary material, Fig. 1, and briefly summarized below. The sequence starts with a cleaned silicon-on-insulator (SOI) wafer of thicknesses 68 ± 0.5 and 147 ± 1.7 nm for SOI and buffer oxide (BOX), respectively, as determined by ellipsometric measurements. The PnCs are defined by high-resolution electron beam lithography and etched through the SOI layer using selective Cl_2 Reactive Ion Etching (RIE) plasma. Three different pitches p of 60, 80, and 100 nm are targeted. The openings for the cavities are etched down to the Si substrate using RIE plasma using SF_6/Ar for top Si layer etching and $CF_4/N_2/O_2$ for BOX etching. Afterward, thermal oxidation is performed in order to grow 12 nm of wet oxide (SiO_2), which is used to protect the SOI layer during the suspension steps. A $CF_4/N_2/O_2$ based RIE plasma then selectively removes the wet SiO_2 grown previously from the cavities' bottom exposing the Si substrate. The Si substrate is then isotropically etched to release the SOI-BOX membrane using XeF_2 gas. The fabrication process is finalized by removing the BOX and wet SiO_2 using hydrofluoric acid in the vaporous phase. Figure 1(c) shows a zoom on the phononic holes at the end of the process. White shells are observed around the holes. By performing atomic force microscopy with a sharp tip on top of the membranes (see the supplementary material, Fig. 2), we reveal that the hole radius on the top surface includes these shells, which are signatures of the non-vertical inner walls in the holes. Statistical analysis of etched PnCs shows that holes have well-defined diameters $2R$ with a standard deviation around 5% of the average diameter, which represents less than 1 nm. It is important to note that the hole radii are modified when changing the pitches (supplementary material, Figs. 2 and 3). In addition, transmission electron microscopy (TEM) cross sections are performed. They indicate that the holes do not fully perforate the membrane [see Fig. 1(d)], having a valley-shape with a depth h larger than 30 nm for the pitch 100 nm and most likely smaller for smaller pitches. A table summarizing all the dimensions is provided in the supplementary material. It is interesting to note that three characteristic lengths can be associated with the complex geometry: t, the neck size in-between holes p-$2R$, and the distance between the bottom of a hole and the bottom of the membrane t - h.

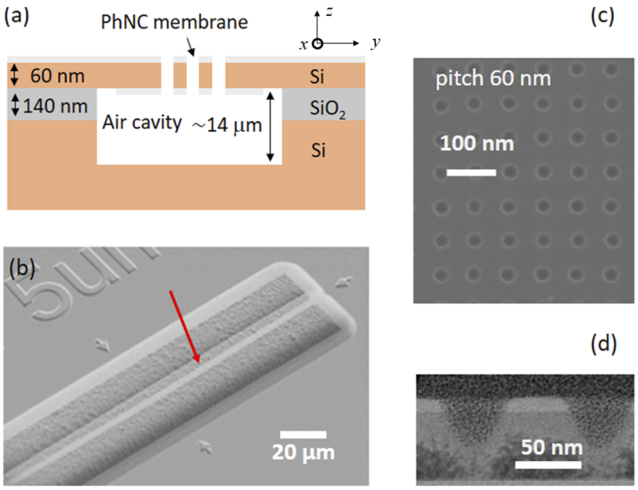

FIG. 1. Phononic membranes investigated. (a) Schematic of the suspended silicon membranes fabricated from silicon-on-insulator samples. (b) SEM image of a membrane strip viewed from the top (red arrow). (c) Zoom on the phononic crystal in the case of a pitch of 60 nm. (d) Cross-section obtained by transmission electron microscopy (different batch, before final top oxide etching) for a phononic membrane of pitch 100 nm.

The membranes are characterized thermally by SThM. This technique is based on atomic force microscopy and involves a thermal sensor in the tip.[30] We use a Wollaston-microwire SThM probe, which consists in a $Pt_{90}Rh_{10}$ metallic-alloy filament of ~200 μm in length bent in a V-shape. The diameter of the filament is about 5 μm (see the supplementary material, Fig. 3, for a photograph of the PtRh sensor). Note that these sizes are close to those of the membrane. The SThM probe is self-heated through Joule effect by passing a current in the filament. The filament average temperature rise $\Delta T = T - T_0$ is determined by inserting it in a Wheatstone bridge, which allows fine measurements of electrical resistance variations. The probe electrical resistance depends on temperature,

$$R = R_0(1 + \alpha \cdot \Delta T), \tag{1}$$

where R_0 is the electrical resistance in the absence of Joule heating at room temperature T_0 and $\alpha = 1.66 \times 10^{-3}$ K^{-1} is the temperature coefficient of the electrical resistance (TCR). A key point is that ΔT decreases when the tip reaches a region where heat can be dissipated more efficiently into the sample. The temperature rises resulting from scans along the membranes performed under ambient conditions are shown in Fig. 2. Large plateaus can be observed close to

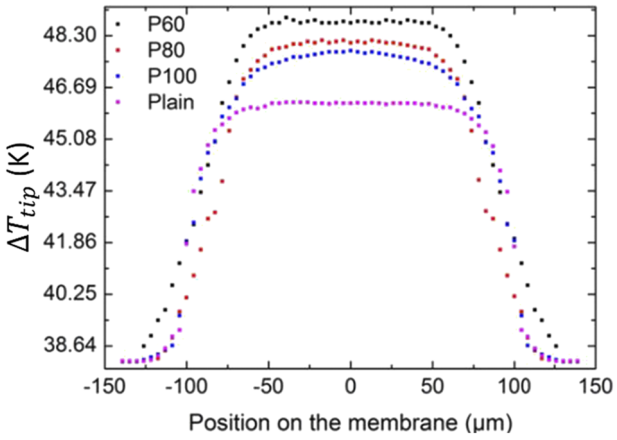

FIG. 2. SThM probe temperature rise according to the position along a membrane for three periodicities (P, in nm) and a reference plain membrane.

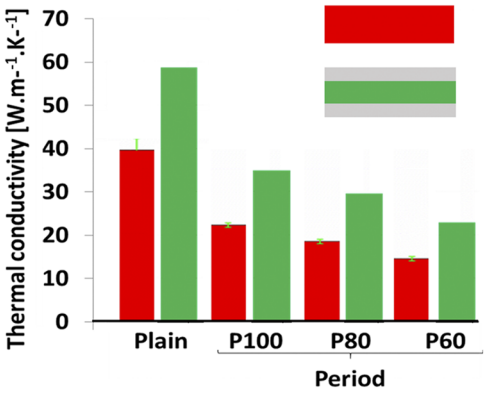

FIG. 3. Effective thermal conductivity of the suspended membranes. Red: thermal conductivity assumed isotropic and not accounting for the presence of a native oxide layer at each side of the membrane. Green: Thermal conductivity of the inner part of the membrane assumed coated with 1.5 nm oxide layer at each side.

the membrane centers indicating a fin-like behavior, which is associated with heat losses in air for the membrane top surface and an exchange through air with the substrate below (thermal radiation is negligible).[24] The plain membrane dissipates the most, and decreasing the pitch induces an increase of the temperature. This means that the membranes with the smallest pitches are thermally more resistive, in agreement with the picture that the surface-to-volume ratio in these objects is larger and that the phonon effective mean free path is reduced accordingly. The thermal conductivity of the membranes is determined from the plateau values (Fig. 2) according to a method involving (i) a splitting of the heat transfer contributions due to air and due to contact in the SThM-probe average temperature variation, (ii) a calibration based on bulk materials, and (iii) FEM simulation of the whole geometry, where the membrane is considered as a single material. This method is described in detail in a previous publication.[24]

The effective thermal conductivities of the membranes, considered isotropic, are found to range between 40 and 15 W m^{-1} K^{-1} (red bars in Fig. 3), which is between 3.7 and 10 times smaller than the bulk value (λ_{bulk} = 148 W m^{-1} K^{-1}). It was shown in Ref. 24 that SThM performed in ambient conditions probes both in-plane and cross-plane heat conduction. While in-plane thermal conductivity is often probed under vacuum condition, cross-plane heat conduction is affected by the presence of the native oxide. Considering the two layers at each side of the membrane, the value of the inner part made only of silicon, supposed isotropic, is found to range between ~60 and 23 W m^{-1} K^{-1}, which is 2.5 to 6.4 times smaller than the bulk value (green bars in Fig. 3). The holes, therefore, decrease thermal conductivity by a factor ~2.5, in addition to the 2.5 factor associated with thickness reduction. This value shows that nanostructuring allows reducing the effective thermal conductivity, but not necessarily with a factor as large (~85 in Ref. 14) as suggested by other works. In addition, reducing the thickness may be simpler than obtaining complex shapes.

We now turn to a numerical analysis. For unperforated membranes, the in-plane thermal conductivity can be calculated semi-analytically with the Casimir–Fuchs–Sondheimer (CFS) model,[33–36] which considers that diffuse reflections by boundaries can reduce the apparent free path in a confined geometry. Indeed, such reflections with the top and bottom surfaces essentially extinguish phonons, since they have equal probability to be scattered along the gradient /membrane direction or in the opposite direction (diffuse reflection induces a cosine distribution law for the phonon packets departing from the surface, which is maximal at the normal to the surface). For structural elements that do not have such equal probability, such as surfaces of the holes that are not parallel to the gradient direction, the path of the phonons is to be followed until they reach their bulk mean free path. We extend the CFS theory by averaging the mean free path in the membrane. The reduction factor F for the spectral thermal conductivity is computed from the projection of the average free path along the gradient direction (here y) for a membrane of thickness t and unit cell of period p,

$$F(\Lambda) = \frac{3}{2\pi \cdot f \cdot p^2 t \cdot \Lambda_0} \int_{-\frac{p}{2},-\frac{p}{2},-\frac{t}{2},}^{\frac{p}{2},\frac{p}{2},\frac{t}{2},} \mathrm{d}x\mathrm{d}y\mathrm{d}z V(x,y,z) \times \int_0^{\pi} \mathrm{d}\theta \int_0^{\pi} \mathrm{d}\phi \, \Lambda(x,y,z,\theta,\phi) \sin^2\theta \sin\phi. \quad (2)$$

V is a function that describes the local presence of matter or void ($\int V \mathrm{d}x\mathrm{d}y\mathrm{d}z = f \cdot p^2 t$, where f is the filling fraction), Λ_0 is the bulk mean free path (for silicon its averaged value is 180 nm when accounting only for acoustic modes[26]), and Λ the position- and angle-dependent free path. In the absence of hole (V = 1, $\int V \mathrm{d}x\mathrm{d}y\mathrm{d}z = p^2 t$) Eq. (2) reproduces the CFS model; it further allows observing the impact of the phononic crystal for arbitrary shapes of holes. Monte Carlo sampling is performed for initial phonon position, initial phonon direction (forward direction only), and total distance traveled, according to the bulk mean free path. Directions after diffuse reflections are also selected from Monte Carlo sampling. Examples of phonon paths for fully diffuse or fully specular reflection are provided in the supplementary material (see the video). The numerical results provided in the following consider only diffuse reflections, which is most likely at room temperature. It

is found that many reflections are still due to the membrane sides due to the thinness of the membrane (60 nm) compared with the average mean free path. The reduction factor F depends on the value of the actual bulk mean free path and is given for varying hole shapes in Fig. 4. It can be seen that paraboloids decrease the free paths less efficiently (curves are located very close) than fully perforating cylinders, the latter being able to reduce the effective mean free path by a factor two with respect to the pristine membrane around 100 nm.

One of the reasons for the decrease in mean free path is the possibility of backscattering of the phonons, as underlined by the shape of the distribution shown in the inset of Fig. 4. Note that backscattering cannot be predicted if the first scattering event with a hole is assimilated to extinction as in the CFS usual model and previous phonon ray-tracing treatments.[37] The shape of the distribution of free paths (projected along the gradient direction) is therefore modified with a more-pronounced peak, as shown for nanowires in Ref. 38. For paraboloidal holes, the backscattering effect is weaker and local free paths are positive, albeit reduced, behind the holes, as shown by the position-dependent free path map of Fig. 5(a) (see the supplementary material for the case of perforating holes). It is also enlightening to analyze the direction dependence of the free path distribution. Some directions are found to favor the transport in Fig. 5(b), for instance, those parallel to the membrane surface and keeping away from the holes. This feature was exploited by the Nomura group to create staggered crystals, which are less favorable for heat transport.[20] It is important to note that phonons transported cannot be distributed homogeneously after their free paths [Fig. 5(a)], which probably induces local nonequilibrium distribution.[39] In our model based on CFS, strong local nonequilibrium inhomogeneities are not accounted for. To analyze the transport beyond such approximation, a full Monte Carlo spatial scheme would be needed.[8,39–41]

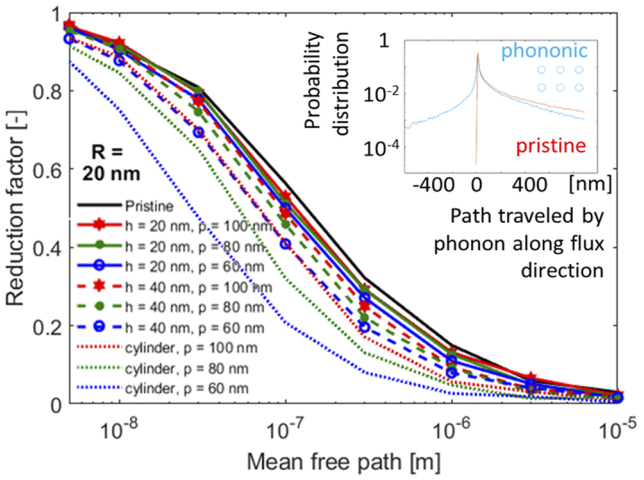

FIG. 4. Reduction factor for in-plane thermal conductivity in membranes for various periodicities p and hole depths h. The paraboloidal holes have a maximal radius R = 20 nm. Inset: Probability for a phonon to travel a certain distance along the flux direction in the case of a perforating cylindrical hole.

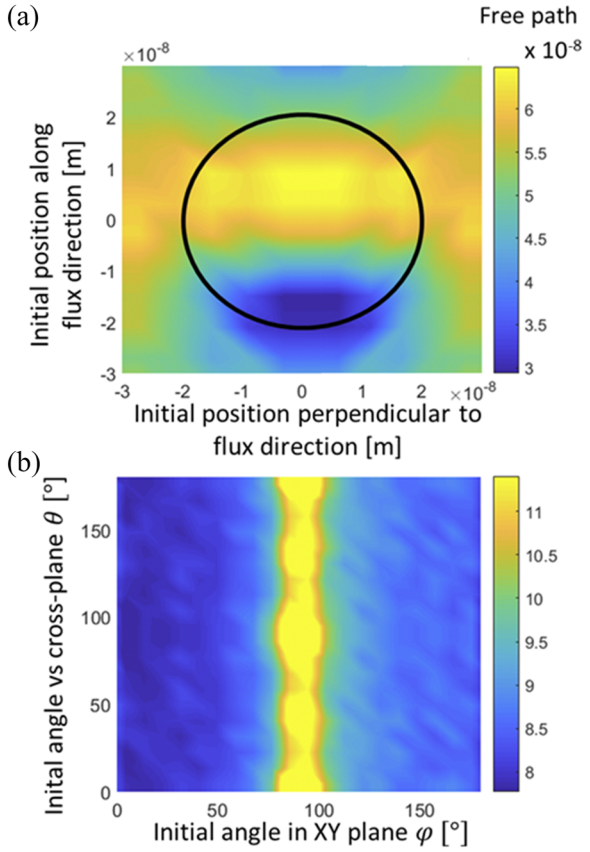

FIG. 5. Phonon free paths as a function of initial position and direction in the case of paraboloidal holes with mean free path 200 nm (R = 20 nm, h = 40 nm). (a) Average distance traveled in the flux direction (y) as a function of initial position in the (x,y) plane. The circle underlines the position of the hole. (b) Average distance traveled as a function of initial angle.

The last ingredient missing for computing the in-plane thermal conductivity in the membranes is the mean free path distribution $d\lambda/d\Lambda$ in silicon bulk,[45,46]

$$\lambda_{membrane} = \int_{\Lambda=0}^{\infty} \frac{d\lambda}{d\Lambda} F(\Lambda) d\Lambda. \quad (3)$$

Many works aimed at determining this distribution $d\lambda/d\Lambda$. Some theoretical ones are based on the knowledge of relaxation times and require inputs related to the phonon dispersion such as heat capacity and group velocity $(c_p(\omega), v_g(\omega))$, while other works do not need prior knowledge of dispersion. Regularization of ill-posed inverse problem can be required, and there is still uncertainty with respect to the actual distribution. As a result, we tested various mean free path (MFP) distributions,[40,42–44] as shown in Fig. 6 (light full lines—see the supplementary material, Sec. 5, for more details on the distributions considered). In the following, we consider that thermal conductivity in the membrane is isotropic, since the experimental value was determined for an equivalent isotropic material. This allows comparing equivalent quantities. Note also that prediction of the cross-plane contribution depends on many

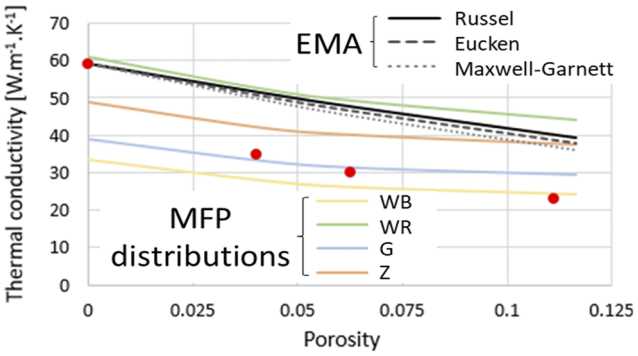

FIG. 6. Thermal conductivity vs porosity (void fraction). Experimental data (red dots) are compared with effective medium approximations accounting for reduction of mean free path in pristine membranes and full computations, including mean free path distributions, taken from models WB,[42] WR,[40] G,[43] or based on experimental data Z.[44]

unknown parameters related to the native oxide. The four tested distributions provide all values close to that found experimentally, but with a slope vs porosity that seems less steep. We speculate that the difficulty in reproducing the exact experimental trend with the models is due to the local phonon nonequilibrium observed in Fig. 5. Another reason could be some anisotropy of thermal conductivity. Interestingly, all the model slopes are less steep than those of different effective medium approximations (EMA, see the supplementary material, Sec. 6), given by the black lines. In these models, the thermal conductivity of the host medium is assimilated to the pristine membrane one as in Ref. 22. An interesting point is that the experimental thermal conductivities of the holey membranes are well below the EMA predictions, demonstrating that the actual shape of the hole is important and that ballistic thermal transport takes place at the local scale. Note that this was not necessary the case for some data reported for thermophononic crystals in the past,[47] since some works included objects with sizes larger than the average bulk mean free path.

In conclusion, we have measured the thermal conductivity of partially perforated phononic membranes. These structures could be useful as more stable than fully perforated membranes. A porosity only slightly larger than ~12% allows for reducing thermal conductivity by a factor 2.5 with respect to the membrane, leading to a factor 6 reduction in comparison with the bulk. Thermal conductivity decreases in a more pronounced way than predictions of effective medium approximations, and the pore shape influences the thermal conductivity, which is a feature that is not captured by the reduced mean free path approach. The exact paths traveled by thermal phonons in sub-mean free path size objects is therefore key for determining effective heat-conduction properties.

See the supplementary material for further information about the fabrication process, the hole shape characterization, an image of SThM scanning on a membrane, the Monte Carlo computing of the mean free paths, the mean free path distributions tested, and the considered effective medium approximations. Video samples of the phonon paths are also provided.

The authors acknowledge support from INSA Lyon through BQR project MaNaTherm, EU projects QuantiHeat and ERC (Grant No. UPTEG 338179), ANR project NanoHeat, and Project NANO2017. This work was partly supported by the STMicroelectronics-IEMN common laboratory and the RENATECH French network. The authors thank Dr. S. Gomes and Dr. S. Lefevre for useful discussions and R. Bon and F. Andre for the TEM images. The authors also thank Dr. T. Skotnicki for discussions.

AUTHOR DECLARATIONS

Conflict of Interest

The authors have no conflicts to disclose.

Author Contributions

A.M.M., V.L., and M.H. contributed equally to this work.

DATA AVAILABILITY

The data that support the findings of this study are available from the corresponding authors upon reasonable request.

REFERENCES

[1] D. Li, Y. Wu, P. Kim, L. Shi, P. Yang, and A. Majumdar, Appl. Phys. Lett. **83**, 2934 (2003).
[2] J. A. Johnson, A. A. Maznev, J. Cuffe, J. K. Eliason, A. J. Minnich, T. Kehoe, C. M. S. Torres, G. Chen, and K. A. Nelson, Phys. Rev. Lett. **110**, 025901 (2013).
[3] J. Cuffe, O. Ristow, E. Chávez, A. Shchepetov, P.-O. Chapuis, F. Alzina, M. Hettich, M. Prunnila, J. Ahopelto, T. Dekorsy, and C. M. Sotomayor Torres, Phys. Rev. Lett. **110**, 095503 (2013).
[4] Y. S. Ju and K. E. Goodson, Appl. Phys. Lett. **74**, 3005 (1999).
[5] J. Ravichandran, A. K. Yadav, R. Cheaito, P. B. Rossen, A. Soukiassian, S. J. Suresha, J. C. Duda, B. M. Foley, C.-H. Lee, Y. Zhu, A. W. Lichtenberger, J. E. Moore, D. A. Muller, D. G. Schlom, P. E. Hopkins, A. Majumdar, R. Ramesh, and M. A. Zurbuchen, Nat. Mater. **13**, 168 (2014).
[6] M. N. Luckyanova, J. Garg, K. Esfarjani, A. Jandl, M. T. Bulsara, A. J. Schmidt, A. J. Minnich, S. Chen, M. S. Dresselhaus, Z. Ren, E. A. Fitzgerald, and G. Chen, Science **338**, 936 (2012).
[7] J.-S. Heron, C. Bera, T. Fournier, N. Mingo, and O. Bourgeois, Phys. Rev. B **82**, 155458 (2010).
[8] W. Park, G. Romano, E. C. Ahn, T. Kodama, J. Park, M. T. Barako, J. Sohn, S. J. Kim, J. Cho, A. M. Marconnet, M. Asheghi, A. M. Kolpak, and K. E. Goodson, Sci. Rep. **7**, 6233 (2017).
[9] Y. Benveniste, J. Appl. Phys. **61**, 2840 (1987).
[10] C.-W. Nan, R. Birringer, D. R. Clarke, and H. Gleiter, J. Appl. Phys. **81**, 6692 (1997).
[11] T. Vasileiadis, J. Varghese, V. Babacic, J. Gomis-Bresco, D. Navarro Urrios, and B. Graczykowski, J. Appl. Phys. **129**, 160901 (2021).
[12] M. Maldovan, Nature **503**, 209 (2013).
[13] A. M. Marconnet, T. Kodama, M. Asheghi, and K. E. Goodson, Nanoscale Microscale Thermophys. Eng. **16**, 199 (2012).
[14] J. Tang, H.-T. Wang, D. H. Lee, M. Fardy, Z. Huo, T. P. Russell, and P. Yang, Nano Lett. **10**, 4279 (2010).
[15] J.-K. Yu, S. Mitrovic, D. Tham, J. Varghese, and J. R. Heath, Nat. Nanotechnol. **5**, 718 (2010).
[16] P. E. Hopkins, C. M. Reinke, M. F. Su, R. H. Olsson, E. A. Shaner, Z. C. Leseman, J. R. Serrano, L. M. Phinney, and I. El-Kady, Nano Lett. **11**, 107 (2011).

[17] E. Dechaumphai and R. Chen, J. Appl. Phys. **111**, 073508 (2012).
[18] J. Maire, R. Anufriev, R. Yanagisawa, A. Ramiere, S. Volz, and M. Nomura, Sci. Adv. **5**, e1700027 (2017).
[19] N. Zen, T. A. Puurtinen, T. J. Isotalo, S. Chaudhuri, and I. J. Maasilta, Nat. Commun. **5**, 3435 (2014).
[20] R. Anufriev, A. Ramiere, J. Maire, and M. Nomura, Nat. Commun. **8**, 15505 (2017).
[21] R. Anufriev and M. Nomura, Mater. Today Phys. **15**, 100272 (2020).
[22] A. Minnich and G. Chen, Appl. Phys. Lett. **91**, 073105 (2007).
[23] A. M. Massoud, P.-O. Chapuis, B. Canut, and J.-M. Bluet, J. Appl. Phys. **128**, 175109 (2020).
[24] A. M. Massoud, J.-M. Bluet, V. Lacatena, M. Haras, J.-F. Robillard, and P.-O. Chapuis, Appl. Phys. Lett. **111**, 063106 (2017).
[25] V. Lacatena, M. Haras, J.-F. Robillard, S. Monfray, T. Skotnicki, and E. Dubois, Microelectron. Eng. **121**, 131 (2014).
[26] W. Cheng, A. Alkurdi, and P.-O. Chapuis, Nanoscale Microscale Thermophys. Eng. **24**, 150 (2020).
[27] S. Neogi, J. S. Reparaz, L. F. C. Pereira, B. Graczykowski, M. R. Wagner, M. Sledzinska, A. Shchepetov, M. Prunnila, J. Ahopelto, C. M. Sotomayor-Torres, and D. Donadio, ACS Nano **9**, 3820 (2015).
[28] B. Graczykowski, A. El Sachat, J. S. Reparaz, M. Sledzinska, M. R. Wagner, E. Chavez-Angel, Y. Wu, S. Volz, Y. Wu, F. Alzina, and C. M. Sotomayor Torres, Nat. Commun. **8**, 415 (2017).
[29] M. Nomura, J. Nakagawa, Y. Kage, J. Maire, D. Moser, and O. Paul, Appl. Phys. Lett. **106**, 143102 (2015).
[30] S. Gomès, A. Assy, and P.-O. Chapuis, Phys. Status Solidi A **212**, 477 (2015).
[31] J. Lee, W. Lee, G. Wehmeyer, S. Dhuey, D. L. Olynick, S. Cabrini, C. Dames, J. J. Urban, and P. Yang, Nat. Commun. **8**, 14054 (2017).
[32] M. Haras, V. Lacatena, T. M. Bah, S. Didenko, J.-F. Robillard, S. Monfray, T. Skotnicki, and E. Dubois, IEEE Electron Device Lett. **37**, 1358 (2016).
[33] H. B. G. Casimir, Physica **5**, 495 (1938).
[34] J. Ziman, "Electrons and phonons," in *The Theory of Transport Phenomena in Solids*, 2001st ed. (Oxford University Press, 1961).
[35] K. Fuchs, Math. Proc. Cambridge Philos. Soc. **34**, 100 (1938).
[36] E. H. Sondheimer, Adv. Phys. **1**, 1 (1952).
[37] A. Jain, Y.-J. Yu, and A. J. H. McGaughey, Phys. Rev. B **87**, 195301 (2013).
[38] R. Anufriev, S. Gluchko, S. Volz, and M. Nomura, ACS Nano **12**, 11928 (2018).
[39] Q. Hao, D. Xu, H. Zhao, Y. Xiao, and F. J. Medina, Sci. Rep. **8**, 9056 (2018).
[40] B. T. Wong, M. Francoeur, and M. Pinar Mengüç, Int. J. Heat Mass Transfer **54**, 1825 (2011).
[41] D. Lacroix, K. Joulain, and D. Lemonnier, Phys. Rev. B **72**, 064305 (2005).
[42] A. Ward and D. A. Broido, Phys. Rev. B **81**, 085205 (2010).
[43] J. V Goicochea, M. Madrid, and C. Amon, J. Heat Transfer **132**, 102401 (2010).
[44] L. Zeng, K. C. Collins, Y. Hu, M. N. Luckyanova, A. A. Maznev, S. Huberman, V. Chiloyan, J. Zhou, X. Huang, K. A. Nelson, and G. Chen, Sci. Rep. **5**, 17131 (2015).
[45] A. J. Minnich, Phys. Rev. Lett. **109**, 205901 (2012).
[46] F. Yang and C. Dames, Phys. Rev. B **87**, 035437 (2013).
[47] M. Nomura, Y. Kage, J. Nakagawa, T. Hori, J. Maire, J. Shiomi, R. Anufriev, D. Moser, and O. Paul, Phys. Rev. B **91**, 205422 (2015).